Influence of orbital contributions to the valence band alignment of Bi_2O_3, Fe_2O_3, $BiFeO_3$, and $Bi_{0.5}Na_{0.5}TiO_3$

Shunyi Li,* Jan Morasch, and Andreas Klein
Technische Universität Darmstadt, Institute of Materials Science, Surface Science Division, Petersenstrasse 32, 64287 Darmstadt, Germany

Christina Chirila and Lucian Pintilie
National Institute of Materials Physics, Atomistilor 105bis, Magurele, 077125, Romania

Lichao Jia and Klaus Ellmer
Helmholtz-Zentrum Berlin für Materialien und Energie, Institute Solar Fuels, Hahn-Meitner-Platz 1, 14109 Berlin, Germany

Michael Naderer and Klaus Reichmann
Technische Universität Graz, Christian Doppler Laboratory for Advanced Ferroic Oxides, Stremayrgasse 9, A-8010 Graz, Austria

Melanie Gröting and Karsten Albe
Technische Universität Darmstadt, Institute of Materials Science, Materials Modelling Division, Petersenstrasse 32, 64287 Darmstadt, Germany

(Received 14 June 2013; published 17 July 2013)

The formation of an interface between Bi_2O_3, Fe_2O_3, $BiFeO_3$, $Bi_{0.5}Na_{0.5}TiO_3$, and the high work function metallic RuO_2 is studied using photoelectron spectroscopy with *in situ* RuO_2 deposition. Schottky barrier heights are derived and the valence band maximum energies of the studied materials are aligned with respect to each other as well as to other functional oxides like $SrTiO_3$ and $PbTiO_3$. The energy band alignment follows systematic trends compared to a large number of oxides, and can be understood in terms of the contribution of Fe $3d$ and Bi $6s/6p$ (lone pair) orbitals to electronic states near the valence band maximum. The results indicate that the valence band maxima are largely determined by the local environment of the cations, which allows to estimate valence band maximum energies of oxides with multiple cations from those of their parent binary compounds. The high valence band maximum of $BiFeO_3$ is consistent with reported p-type conduction of acceptor doped material, while the high conduction band minimum makes n-type conduction unlikely.

DOI: 10.1103/PhysRevB.88.045428 PACS number(s): 73.30.+y, 77.84.Bw, 79.60.Jv

I. INTRODUCTION

For materials with an energy band gap that separates occupied and unoccupied states, the energies of the valence band maximum (E_{VB}) and conduction band minimum (E_{CB}) determine whether a material can be electrically conducting or not.[1–3] Although the electrical conductivity can often be varied by doping, there are certain doping limits in materials, which is particularly intriguing for those that have energy gaps around 3 eV. This is a typical energy gap of many technologically important oxides. These oxides can be made either n-type by donor doping, such as ZnO, In_2O_3, SnO_2, TiO_2, $SrTiO_3$, and $BaTiO_3$, or p-type by acceptor doping, such as Cu_2O, $CuAlO_2$, and NiO.[4] Ambipolar dopability, which means that a material can be made both n or p type by corresponding doping, as for instance it is possible with GaN, remains rare for oxides. There are also a few materials with energy gaps around 3 eV that remain insulating regardless of doping type. Among them are the Pb- and Bi-based ferroelectric compounds like $Pb(Zr,Ti)O_3$ (PZT) and $Bi_{0.5}Na_{0.5}TiO_3$-$BaTiO_3$ (BNT-BT).[5,6]

When the Fermi level, which determines the electronic carrier concentrations in the valence band (i.e., hole concentration p) and in the conduction band (i.e., electron concentration n), is located well above the E_{VB} or below E_{CB}, the material is an insulator. The variation of the Fermi level position by doping is limited by the formation of intrinsic defects.[1,7–9] Lowering the Fermi energy by acceptor doping generally reduces the formation enthalpy of intrinsic donor defects like oxygen vacancies or metal interstitials.[1] The doping limit, i.e., the lowest possible Fermi energy is reached when the formation enthalpy of the donors becomes zero. Raising the Fermi energy by donor doping is correspondingly limited by intrinsic acceptor formation. Hence the different electrical properties of oxides are related to the energies of the valence and conduction band on an absolute energy scale. A material having low valence band energy cannot become a p-type conductor, while a material having high conduction band energy cannot be an n-type conductor. The best insulators, SiO_2 and Al_2O_3, have large energy gaps (>8 eV) and both low valence band maximum and high conduction band minimum energies.

There are different possibilities to arrange the valence band and the conduction band on an absolute energy scale. Taking the vacuum energy as a reference is often the first choice. With respect to the vacuum energy, the valence band maximum and conduction band minimum are given by the ionization potential ($I_P = E_{VAC} - E_{VB}$) and the electron affinity ($\chi = E_{VAC} - E_{CB}$), respectively. However, due to surface dipole contributions, these quantities depend significantly on the surface orientation and the surface termination.[10] For the n-type transparent conducting oxides ZnO, In_2O_3, and SnO_2 the variation can be up to 1 eV.[11,12]

Valence and conduction band energies can also be derived from electrochemical studies using solid/electrolyte

interfaces.[13] E_{VB} and E_{CB} are determined with respect to the potential of a normal hydrogen electrode (NHE), whose potential corresponds to an energy approximately 4.5 eV below the vacuum level.[14]

A third possibility of aligning the energy bands of materials on an absolute energy scale is by measuring the energy band alignment directly at the intimate contacts between materials.[15] Such measurements can be performed, e.g., using photoelectron spectroscopy and stepwise deposition of a contact material onto a substrate.[16] Using such studies it has been shown that the valence band offsets ΔE_{VB}, i.e., the discontinuity in the valence band maximum energy at the interface, are small for interfaces between oxides where the valence bands are formed almost exclusively from O $2p$ states (e.g., ZnO, In_2O_3, SnO_2, Al_2O_3, $SrTiO_3$).[3,17] Such an alignment is often termed *common anion rule* alignment. Small valence band offsets between materials with common anions are also observed between Zn and Cd chalcogenides.[18,19] The oxides and the chalcogenides have a considerable ionic bonding character in common. The more covalently bonded elemental and III-V semiconductors do not show a common anion band alignment (see, e.g., Ref. 18), which is related to interface dipoles due to a high density of induced interface states.[20–22]

Photoemission studies have further revealed that oxides with cation orbitals contributing to the valence band formation show considerably higher E_{VB}.[2,17,23] For oxides containing Cu, which has a $3d^{10}$ configuration, this can be understood by the hybridization of $3d$ states with O $2p$ states. The resulting upward shift of the valence band maximum is also known for Cu chalcopyrites as p-d repulsion.[24] In contrast, the origin of the ∼1 eV higher valence band maximum of $PbTiO_3$ (PTO) compared to $SrTiO_3$ (STO) is less evident. In PTO, Pb is present as Pb^{2+}, i.e., in a $6s^2$ configuration. The occupied $6s$ orbitals contribute to the valence band density of states. However, due to the relativistic stabilization of the $6s$ electrons,[25] the Pb $6s$ states appear predominantly as a separate energy band below the O $2p$-dominated valence bands.[26,27]

$BiFeO_3$ (BFO) is a wide-gap oxide semiconductor with an energy band gap around 2.8 eV[28–30] and has recently attracted considerable attention due to its multiferroic properties, which means a simultaneous appearance of ferroelectricity and antiferromagnetism.[31–33] This enables a variety of potential applications in the field of data storage, spintronics, and sensor technologies. BFO is a prototype multiferroic compound with the transition from the ferroelectric state to the paraelectric state at $T_C = 830\,^{\circ}C$, and from antiferromagnetic state to the paramagnetic state at $T_N = 370\,^{\circ}C$.[34] The photoelectric effect observed in BFO is also of great research interest due to the potential applications in photovoltaic or photocatalytic devices.[35–37] The binary oxides Bi_2O_3 and Fe_2O_3 have also been studied for environmental protection and energy conversion with solar energy utilization. Both of them show promising photocatalytic properties, which are attractive for applications such as organic degradation[38–41] and hydrogen generation by photocatalytic water splitting.[42,43] For the latter application, the absolute energies of the valence and conduction band are also of particular relevance as they should embrace the redox potentials for the hydrogen and oxygen evolution reactions.[44]

$Bi_{0.5}Na_{0.5}TiO_3$ (BNT), discovered in the 1960's by Smolensky,[45] is a promising lead-free ceramic material to replace $Pb(Zr,Ti)O_3$ in ferroelectric applications like actuators.[5,6,46] BNT can be described as a complex perovskite with mixed A-site occupation (Bi^{3+}, Na^{+} in twelvefold coordination) and a single cation (Ti^{4+} in sixfold coordination) on the B site. It crystallizes with rhombohedral symmetry[47] and is highly modifiable by doping or the formation of solid solutions with other perovskites like $BaTiO_3$ (BT)[48] or $Bi_{0.5}K_{0.5}TiO_3$ (BKT).[49] The mixture with tetragonal perovskites such as the mentioned BT and BKT leads to the formation of a morphotropic phase boundary, at which most relevant parameters show maximized values.

In this contribution we study the valence band maximum energies of $BiFeO_3$, its parent oxides Bi_2O_3 and Fe_2O_3, and the lead-free ferroelectric $Bi_{0.5}Na_{0.5}TiO_3$ in order to identify the contribution of occupied $6s$ orbitals to the upward shift of valence band maximum energy. The E_{VB} are determined by measuring their Schottky barrier heights with metallic RuO_2 using photoelectron spectroscopy. The Schottky barrier heights will be compared to those determined recently for $(Ba,Sr)TiO_2$ (BST) and $Pb(Zr,Ti)O_3$.[50,51] The Fermi level in RuO_2 can therefore be used as a reference to compare the absolute energies of E_{VB} and E_{CB} for different oxides by applying transitivity. The transitivity of energy band alignment of oxides using RuO_2 as a reference has already been demonstrated explicitly for $SrTiO_3$ and $PbTiO_3$.[2] Compared to elemental metals, the deposition of RuO_2 does not introduce defects at the oxide surface, which would affect the energy band alignment.[52–55]

II. METHODS

Bi_2O_3 thin films were deposited on commercial $Si(100)/SiO_2/TiO_2/Pt(111)$ wafer by RF reactive sputtering from a 2 inch metallic bismuth target (Alineason Materials Technology). The deposition was carried out at room temperature with a RF power of 50 W in an Ar/O_2 gas mixture, which contains 10% O_2. The deposition time was set to 120 seconds, corresponding to a film thickness of 30 nm, determined by profilometer measurements.

The iron oxide films were prepared by magnetron sputtering in a pure argon atmosphere at a pressure of 0.5 Pa from an oxidic Fe_2O_3 (hematite) target (K. J. Lesker Co.) with the dimensions 51-mm diameter and 4-mm thickness on a copper backing plate. The RF (27.56 MHz) discharge power was 50 W and the layers were deposited onto glass substrates coated with fluorine-doped tin oxide (SnO_2:F) without intentional substrate heating. For a sputtering time of 60 min, a film thickness of about 120 nm was obtained. Besides the strong diffraction peaks from the thick SnO_2:F layer, the XRD pattern shows three weak peaks, which can be assigned to hematite (JCPDS 89-0597). Due to the low substrate temperature, the XRD peaks are weak and broad, indicating a nanocrystalline structure. Using the Scherrer equation, a grain size of about 20 nm can be calculated from the peak width.

The $BiFeO_3$ layer was grown by pulsed laser deposition (PLD) method on single crystalline $SrTiO_3$ substrate with (001) orientation. The substrate was previously cleaned in hydrofluoric acid (HF) buffer solution and then annealed in

air at 1000 °C for 2 hours in order to obtain terraces with step heights of one unit cell. A $SrRuO_3$ (SRO) epitaxial buffer layer has been deposited on the $SrTiO_3$ substrate, acting as a bottom electrode and also as an excellent template for the heteroepitaxial growth of a high-quality ferroelectric perovskite. The SRO film was deposited at a substrate temperature of 700 °C, in a background atmosphere of 0.133-mbar oxygen, with a laser fluence 2 J/cm^2 and a repetition rate of 5 Hz. After the SRO deposition, the temperature was lowered to 670 °C, and the BFO layer was deposited in an oxygen atmosphere of 0.026 mbar, with a laser fluence of 1.2 J/cm^2 and a repetition rate of 10 Hz. A postdeposition annealing was performed in the PLD chamber in full oxygen atmosphere at 390 °C for 1 h. The epitaxial nature of the SRO and BFO layers was confirmed by x-ray diffraction analysis. The thickness of the SRO film was ∼15 nm and that of the BFO film ∼80 nm as determined from x-ray reflectometry.

Samples of $Bi_{0.5}Na_{0.5}TiO_3$ with a Ti deficiency of 2% were prepared via a conventional mixed-oxide method. The Ti deficiency was chosen to ensure a single phase material, since evaporation of Bi_2O_3 and Na_2O during sintering and calcination of stoichiometric BNT leads to nonstoichiometric compositions with an excess of B-site cations, which results in the formation of secondary phase inclusions.[56] As starting materials for the synthesis Bi_2O_3 (99.9% purity, MCP-HEK GmbH), Na_2CO_3 (99.99% purity, Merck), and TiO_2 (99.8% purity, Tronox) were used. All starting materials were dried at 260 °C for 48 h to avoid weighing errors caused by adsorption of humidity. After drying, the materials were cooled and stored in a desiccator over silica gel. The reactants were mixed in ethanol for 24 h using a horizontal ball mill (Germatec UR1400FU EH) using YSZ milling balls with 5-mm diameter. The resulting suspension was dried in a forced fresh air drying oven (Heraeus LUT 6050) at 120 °C. Before calcination, the precipitate was sieved using a test sieve with a mesh size of 500 μm. The calcination took place in an alumina crucible at 800 °C for 5 h. Subsequently, the material was again ball-milled using the same milling parameters as in the first milling step. After another drying step at 120 °C, the fine powder was sieved to an agglomerate size less than 180 μm and mixed with 5% PEG 20 000 (for synthesis, Merck) as a binding agent. Disc shaped samples with 13-mm diameter were pressed with 150 MPa for 5 min. The binder was removed at 350 °C in an open crucible to promote the transport of the binder decomposition products H_2O and CO_2. The crucibles containing the de-bindered samples were then covered with a lid and sintered at 1100 °C for 5 h.

The determination of energy band alignment was realized by using photoelectron spectroscopy with stepwise deposition of RuO_2 onto the different substrate materials.[17] Four interface experiments were performed independently but with identical deposition conditions for RuO_2. DC reactive sputtering from a 2-inch metallic ruthenium target with a power of 50 W was carried out at room temperature in an Ar/O_2 gas mixture containing 7.5% O_2. These deposition conditions lead to stoichiometric metallic RuO_2 films, which exhibit a work function of ∼6.1 eV.[50] RuO_2 deposition and interface analysis were repeatedly performed under ultrahigh vacuum condition at the DArmstadt Integrated SYstem for MATerials research (DAISY-MAT).[3] X-ray photoelectron spectra were recorded with monochromatic Al Kα radiation at an emission angle of 45° and a pass energy of 5.85 eV, which results in a total energy resolution of <4 eV as determined from the Gaussian broadening of the Fermi edge of a sputter-cleaned Ag sample. With this resolution, binding energies of core levels and valence band maxima can typically be determined with an accuracy of <50 and <100 meV, respectively. All binding energies are given with respect to the Fermi level of a sputter-cleaned Ag sample with an accuracy of ∼50 meV.

Except the Bi_2O_3 film, which is prepared *in situ* in the DAISY-MAT system, the other three materials underwent a moderate thermal treatment in the deposition chamber at 400 °C in pure O_2 (0.1 Pa) in order to remove surface adsorbates. XP-spectra were taken both before and after heating the sample to exclude any chemical change caused by this thermal treatment and to ensure removal of adventitious carbon on the surfaces of the air-exposed samples.

On $BiFeO_3$, Fe_2O_3, and Bi_2O_3 thin films no surface charging was observed during the XPS measurements, because they all have a relatively low film thickness and are deposited on conductive substrates. The $Bi_{0.5}Na_{0.5}TiO_3$ ceramic pellet showed surface charging, which prevented the measurement of the valence band. In order to reduce this disturbance to the Schottky barrier determination, the interface experiment on BNT was carried out with a structured RuO_2/Pt bilayer having an uncovered circle in the center on the top surface of the BNT pellet. This procedure has already been applied successfully before to determine the barrier height at a PZT/RuO_2 interface.[57] The surface charging during XPS measurement disappeared after the RuO_2 reached a film thickness of ∼1 nm due to the formation of a conducting layer at the surface.

The partial density of states of $Bi_{0.5}Na_{0.5}TiO_3$ was calculated using *ab initio* calculations as implemented in the Vienna *ab initio* simulation package (VASP).[58–61] Projector augmented plane waves[62,63] were utilized with the LDA exchange correlation functional,[64] a plane-wave energy cutoff of 800 eV was chosen, and a 16 × 16 × 16 -centered Monkhorst-Pack k-point[65] mesh for the primitive cell (one formula unit ABO_3) was used for Brillouin zone integration. The valence electron configurations of the PAW data sets were Bi $5d^{10}\,6s^2\,6p^3$, Na $2p^6\,3s^1$, Ti $3s^2\,3p^6\,4s^2\,3d^2$, and O $2s^2\,2p^4$. Calculations were performed for a rock-salt ordered configuration of Bi and Na, which lowers the symmetry from $R3c$ to $R3$ and results in Wyckoff splitting of the sites occupied by Ti and O. The pseudocubic 2 × 2 × 2 nonconventional setting was chosen for calculation. Structural parameters were optimized until residual forces were less than 1 meV/Å.

III. RESULTS

A. Chemical state of the surface

XPS measurements have been carried out before the deposition of RuO_2. The corresponding survey spectra are given in Fig. 1. Except for the measurement of $Bi_{0.5}Na_{0.5}TiO_3$, which was performed with charge neutralization using an electron flood gun, no surface charging was observed during the XPS measurements. The survey spectra show the elements expected for the different materials. The most prominent emissions are the Na 1s, Bi 4f, Fe 2p, and O 1s. No adsorbates

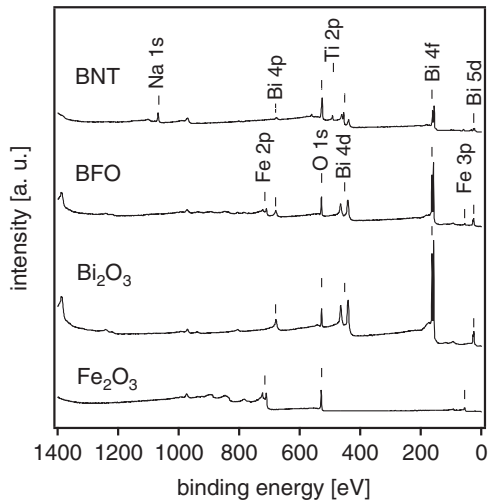

FIG. 1. Survey spectra of Fe_2O_3, Bi_2O_3, $BiFeO_3$, and $Bi_{0.5}Na_{0.5}TiO_3$. The main core level emissions are indicated. No carbon signals (~286 eV) are observed.

such as carbon or any other unexpected species are observed. This indicates surfaces free of contamination and complete removal of adsorbates by the thermal treatment. This is further supported by the absence of hydroxide/water emission in the O 1*s* spectra shown in Fig. 2, which typically occur at 532 eV binding energy.[66] The relative atomic concentrations of individual elements are reflected by the peak intensities. While Bi_2O_3 and Fe_2O_3 show the most intensive Bi and Fe core level emissions, respectively, the corresponding emissions from $BiFeO_3$ are lower, due to the lower concentration of atoms. The intensities of the Bi peaks from BNT are even lower in comparison with BFO as expected, because the A-site cation position in BNT is equally shared by Bi and Na.

High-resolution core level spectra of Bi 4*f*, Fe 2*p*, and O 1*s* emissions are shown in Fig. 2. The binding energies of the Bi 4*f* and O 1*s* core levels are determined by extracting the background intensity with the Shirley function and fitting the resulting curves with Voigt profiles. This background

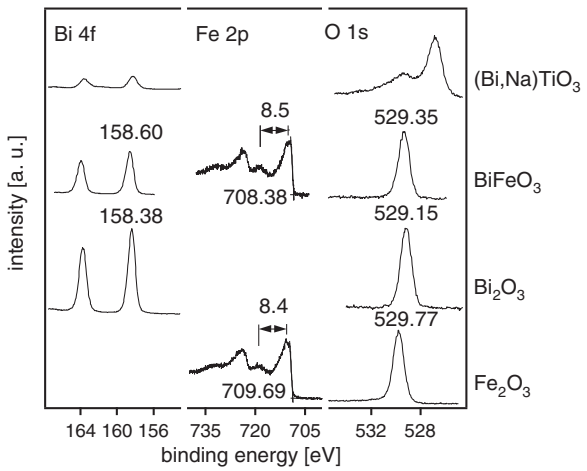

FIG. 2. High-resolution core level spectra of Fe_2O_3, Bi_2O_3, $BiFeO_3$, and $Bi_{0.5}Na_{0.5}TiO_3$. The spectra of BNT has been recorded with an electron flood gun to compensate charging effects.

subtraction does not provide reasonable results for the Fe 2*p* emission because of its broad and asymmetric line shape. The broadening of Fe 2*p* emission is due to multiplet splitting caused by unpaired valence electrons, resulting in an exchange interaction which affects the remaining spin-up and spin-down core electrons differently.[67,68] McIntyre *et al.* have shown that the structure of the surrounding environment also influences the splitting of the Fe 2*p* peak.[69] In principle, curve fitting with multiple peaks can be applied to the Fe 2*p* emission in order to obtain a binding energy. However, curve fitting does not always lead to reproducible and unambiguous results, since different combinations of binding energy and intensity ratios can generate very similar envelopes of the total intensity. Instead, we evaluate a relative energy position of Fe 2*p* emission by extrapolating the emission edge at the low binding energy side of the Fe $2p_{3/2}$ peak to the background intensity. This onset of the Fe $2p_{3/2}$ emission provides a reproducible relative value for the binding energy of the Fe 2*p* peak, as the line shape does not change in the course of the RuO_2 deposition. For the determination of the band alignment, any reproducible relative binding energy will be adequate.

The Bi 4*f* and O 1*s* spectra from both $BiFeO_3$ and Bi_2O_3 exhibit a sharp and symmetric line shape, showing that Bi in both films is in a well-defined chemical environment. This implies a full oxidation of Bi in Bi_2O_3 during reactive sputtering. Comparing the Bi 4*f* and O 1*s* emissions of BFO and Bi_2O_3 reveals almost identical shapes and widths. The binding energy difference between the Bi 4*f* and the O 1*s* peak agrees within 100 meV for the two materials. The asymmetry of the BNT spectra is caused by an imperfect compensation of the charging effect by the electron flood gun. Despite the asymmetry, the peaks are still dominated by emissions having widths comparable to those of the corresponding emissions in the other compounds.

The Fe 2*p* spectra of $BiFeO_3$ and Fe_2O_3 show very similar peak characteristics. The binding energy difference between the Fe 2*p* and the O 1*s* emission is identical for both materials. The maximum of the Fe $2p_{3/2}$ emission occurs at a binding energy ~710 eV, as expected for Fe^{3+}, the nominal oxidation state Fe in both compounds. The +III oxidation state is further supported by the characteristic satellite emission at ~8.5 eV higher binding energy compared to the maximum of the Fe $2p_{3/2}$ emission.[70,71] The width of the Fe $2p_{3/2}$ peak from both compounds is around 3.3 eV, which is lower than the values between 3.8–4.5 eV reported for pure Fe_2O_3 in the literature.[67,70,72] This provides sufficient evidence that the Fe 2*p* emission of both compounds relates to a well-defined +III oxidation state.

B. Valence band spectra

X-ray excited valence band spectra of Fe_2O_3, Bi_2O_3, $BiFeO_3$, and $Bi_{0.5}Na_{0.5}TiO_3$ are shown in Fig. 3. The spectra for Fe_2O_3, Bi_2O_3, and BFO exhibit distinct features as indicated by vertical lines and valence band maximum energies ($E_F - E_{VB}$) of 1.1–1.4 eV. The latter are determined by the interception of the linearly extrapolated valence band edge and the background intensity.

The valence band of Fe_2O_3 has an energy width of ~8.2 eV and shows three fine features at the binding energies around

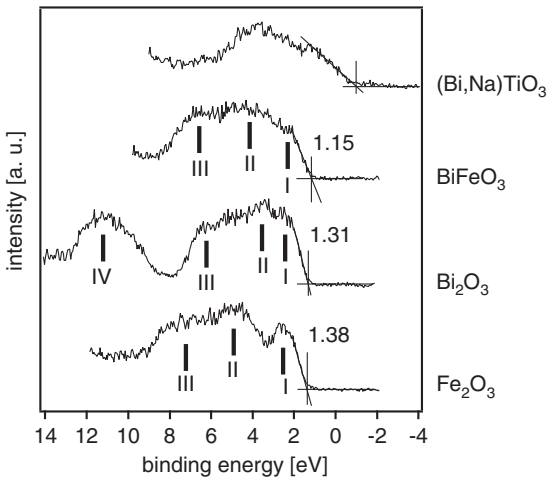

FIG. 3. Valence band spectra of Fe_2O_3, Bi_2O_3, $BiFeO_3$, and $Bi_{0.5}Na_{0.5}TiO_3$. The latter has been recorded with an electron flood gun to compensate charging effects. The energies of the valence band maximum are determined by the interception of the linearly extrapolated valence band edge and the background. The negative binding energy of the BNT valence band maximum is caused by an overcompensation of the charging by the flood gun.

2.5[I], 4.9[II], and 7.2 eV [III], respectively. The relative distance of these energy positions is in good agreement with the reported values on powder,[69] thin film,[71] and single crystal Fe_2O_3 samples.[73] The small deviation of absolute energy positions may be caused by differences in spectral resolution, sample preparation and, most importantly, different references for the alignment of the spectra by different authors. For oxides with valence bands formed primarily by O $2p$ state, the spectrum shows typically two features with an energy separation of $\sim$2 eV with an intensity ratio of 5 : 3. The width of the valence band also extends to only $\sim$6 eV (see, for example Fig. 5, in Ref. 54). However, the valence band of Fe_2O_3 in Fig. 3 clearly exhibits three features with a larger energy separation and a smaller intensity difference. The width of the valence band is also larger compared to that of most oxides. This result is well consistent with DFT calculations[74] and confirms that the electronic states of Fe $3d$ and O $2p$ are strongly hybridized.

The valence band of Bi_2O_3 exhibits also a structure with three features at binding energies of 2.4 [I], 3.5 [II], and 6.2 eV [III] and a well separated peak at about 11.2 eV [IV]. The peak at $\sim$11 eV binding energy is related to the band dominated by Bi $6s$ states, while the upper valence band features I-III are mostly O $2p$ states hybridized with Bi $6s/6p$.[26,75] The spectra confirm that the valence band in Bi_2O_3 is different from those of oxides with valence bands formed predominantly by O $2p$ states. In particular, a contribution of Bi states is expected at the valence band maximum.

The valence bands of $BiFeO_3$ are essentially a mixture of the valence bands of Bi_2O_3 and Fe_2O_3. The energy width of the main valence band emission is slightly smaller than that of Fe_2O_3 but larger than that of Bi_2O_3. The features I, II, and III are broadened due to the mixing while the energy positions lie approximately in between those of the binary oxides. Although the spectrum from 10–14 eV were not included in the measurement, the valence band of $BiFeO_3$ is expected to show also a separate peak in this energy range, originating from the Bi $6s$ states like in Bi_2O_3.[74]

The spectrum of the $Bi_{0.5}Na_{0.5}TiO_3$ could only be measured using an electron flood gun to compensate for charging effects. As it is often the case in such a situation, the spectra are slightly smeared and no quantitative binding energies can be extracted. The latter is evident from the negative binding energy of the valence band maximum, which is caused by an overcompensation of the charging effects. Nevertheless, the binding energy difference between the valence band maximum and the Bi $4f_{7/2}$ emission, which is required for the quantitative determination of the Schottky barrier height below, can be evaluated with almost the same accuracy as for the other materials. This is inferred from the line shape of the Bi $4f$ emission (see Fig. 2), which is dominated by a symmetric line shape which is only $\sim$0.1 eV broader than that of Bi_2O_3 and Fe_2O_3.

C. Interface formation with RuO_2

The investigation of energy band alignment has been performed in four separate interface experiments with RuO_2 as the contact material. During the experiments RuO_2 was stepwise deposited onto Bi_2O_3, Fe_2O_3, BFO, and BNT using identical deposition conditions and comparable thickness increments. The experiments were concluded after complete attenuation of the substrate emissions. The spectra showing the gradual changes of the core levels during interface formation are presented in Fig. 4. The most intense core level peaks, namely Bi $4f$, Fe $2p$, O $1s$, Na $1s$, Ti $2p$, and Ru $3d$ are recorded during the experiments. Due to the similarity of Ru $3d$ spectra[50,51,57] only those from the deposition onto BFO are shown here exemplarily.

Special care was taken during the experiment on BNT because of the surface charging. In order to reduce the charging effect, an electron flood gun was used at the beginning of the measurement before the RuO_2 deposition. All the peaks have rather low binding energies (see discussion of valence bands above) and show a small additional component at higher binding energies. The peak shapes are attributed to an inhomogeneous charging and the too low binding energies to a slight overcompensation of the charging effect. After the first RuO_2 deposition, the XPS measurements of the BNT sample were performed without charge compensation. The charging causes a 11–12 eV shift of all emissions to higher binding energy for a RuO_2 thickness of $\sim$0.4 nm, which is manually removed in Fig. 4 for clarity. As soon as the film thickness reaches $\sim$0.9 nm, all the spectra shift back to lower binding energies and sharp line shapes are observed for all core level emissions. This is a clear indication that the RuO_2 has formed a continuous layer across the surface of sufficient conductivity to avoid charging.

Except the first two measurements on BNT, the spectra from all four samples show a very similar behavior. With increasing RuO_2 thickness, the intensities of all substrate cation emissions (i.e., Bi $4f$, Fe $2p$, Na $1s$, and Ti $2p$) exhibit an exponential decay with relative decay constants corresponding to the different inelastic mean free paths of the individual emissions. This indicates an interface formation with a layer-by-layer

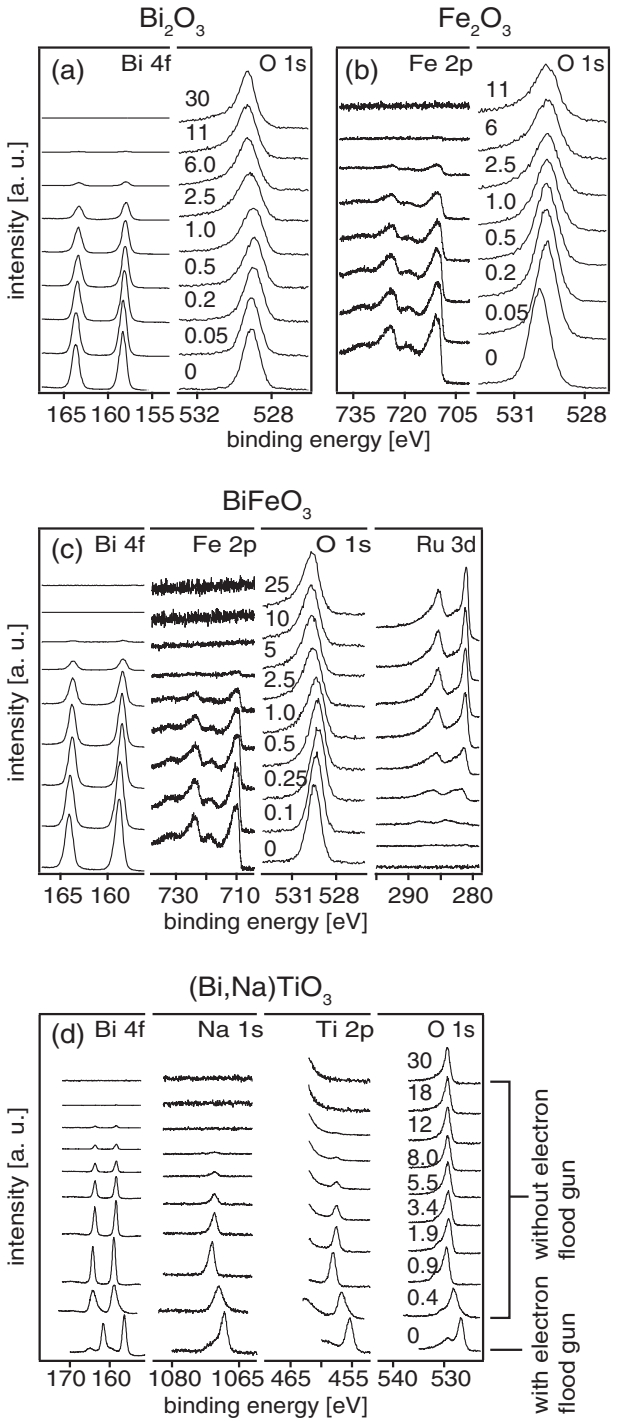

FIG. 4. Core level spectra of (a) Bi_2O_3, (b) Fe_2O_3, (c) BFO, and (d) BNT with stepwise deposition of RuO_2. The ascending film thickness of RuO_2 is indicated beside the O 1*s* spectra correspondingly. The spectra for 0.4 nm RuO_2 thickness on BNT are shifted to lower binding energies for clarity.

growth mode, as already observed for RuO_2 deposition onto (Ba,Sr)TiO_3 and Pb(Zr,Ti)O_3.[50,51,57] Furthermore, the line shapes and widths of the cation emissions do not change with increasing RuO_2 thickness, indicating that the oxidation state does not change. An interface reaction during deposition is therefore excluded. The change in line shape of the O 1*s*

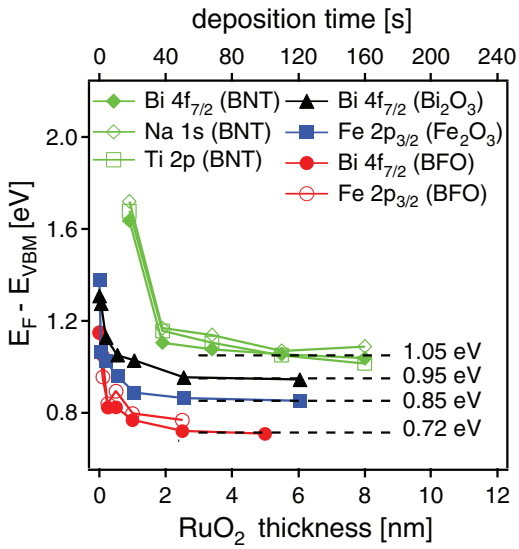

FIG. 5. (Color online) Evolution of the core-level binding-energy shift with increasing RuO_2 film thickness. The distances between core level lines and the valence band maximum energy E_{VB} have been subtracted. The energy values are given with respect to the Fermi level.

emission is due to the transition from the oxygen component of a semiconducting substrate with a symmetric line shape to the oxygen emission of the metallic RuO_2 with an asymmetric Doniach-Sunjic profile.[76] The intensity of the Ru peaks, represented by the Ru 3*d* emission, rises continuously with increasing RuO_2 coverage. The binding energies of the Ru $3d_{5/2}$ emission is 281.0 ± 0.1 eV at the highest film thickness on all substrates, which concurs with recent measurements and literature for RuO_2.[50,51,57,66]

The core level peaks of the cations from the substrates are used for the determination of the binding energy shifts, which reflect directly the evolution of the electrostatic surface potential during RuO_2 deposition. For BFO, both Bi 4*f* and Fe 2*p* emissions are used, while for BNT the Bi 4*f*, Na 1*s*, and Ti 2*p* emissions are used in order to see if they exhibit parallel binding energy shifts. Parallel shifts are required in order to exclude a chemical origin of the shifts. Shifts of the O 1*s* spectra are included only for the first few deposition steps, where the O 1*s* emission is still clearly associated with the substrate and not with the RuO_2 layer.

In Fig. 5, the evolution of the binding energy of the substrate core level lines with increasing thickness of RuO_2 is shown. For better comparison, the differences between core level binding energies and valence band maxima, obtained from the uncoated substrate surfaces, were subtracted for each substrate. Therefore the curves in Fig. 5 can be considered as the evolution of the valence band maximum with respect to the Fermi level. All the curves exhibit a strong downward shift at lower RuO_2 coverage, indicating an upward bending of the valence bands towards the Fermi level. An upward shift corresponds well with the large work function of RuO_2 of 6.1 eV.[50]

Saturation of the binding energy shifts is observed for all four materials after the RuO_2 layer exceeds a thickness of ~2 nm. For $BiFeO_3$ and $Bi_{0.5}Na_{0.5}TiO_3$ a parallel shift of

all core level emissions is observed. $E_F - E_{VB}$ for Bi_2O_3, Fe_2O_3, BFO, and BNT, after saturation of binding energy shifts amount to 0.95, 0.85, 0.72, and 1.05 eV, respectively. The uncertainty is about ±0.1 eV, being slightly larger for BNT due to the uncertainty of the valence band maximum position caused by the charging of the substrate. The values for $E_F - E_{VB}$ correspond directly to the Schottky barriers for holes $\Phi_{B,p}$. By considering the energy gaps of α-Bi_2O_3 (2.5 eV[77]), Fe_2O_3 (2.1 eV[78]), BFO (2.8 eV[28–30]), and BNT (3.3 eV[79]) the barrier heights for electrons at the interface with RuO_2 are derived as $\Phi_{B,n} \approx 1.55$, 1.25, 2.08, and 2.25 eV, respectively. For all four materials, the barrier heights for holes are considerably smaller than those for electrons. A comparable situation is observed for Pb(Zr,Ti)O_3,[2,51] while the Fermi level is closer to the conduction band at the (Ba,Sr)TiO_3/RuO_2 interface. Moreover, the Schottky barrier height for holes deduced for BFO is in good agreement with barrier heights determined from electrical measurements at epitaxial $SrRuO_3$/$BiFeO_3$/Pt capacitors by Pintilie *et al.*[80]

IV. DISCUSSION

For a discussion of the orbital contributions to the valence band maxima and their consequences for the energy band alignment, the crystallographic and electronic structures have to be considered.

A. Crystal structures

Bi_2O_3 has several polymorphs, among which the α and the δ phase are thermodynamically the most stable ones.[81] The crystal structure of α-Bi_2O_3 is monoclinic and belongs to the space group $P2_1/c$ with a fivefold oxygen coordination of the Bi atoms while δ-Bi_2O_3 crystallizes in a cubic structure with space group $Fm\bar{3}m$ and a sixfold oxygen coordination. Due to the highly distorted structure there are different bond lengths between Bi and O in α-Bi_2O_3, ranging from 2.1–3.4 Å (see also Table I).[82,83] δ-Bi_2O_3 possesses a so-called defective fluorite-type lattice, in which only six out of eight anion sites are occupied with oxygen. The Bi-O bond length has been determined using neutron diffraction (ND) as 2.45 Å.[83]

Hematite, i.e., α-Fe_2O_3, has a corundum crystal structure with the space group $R\bar{3}c$. Iron is sixfold coordinated by oxygen atoms in a distorted octahedral environment. There are two different Fe-O bond lengths in the Fe_2O_3 lattice, i.e., $[\text{Fe-O}]_{long} \approx 2.1$ Å and $[\text{Fe-O}]_{short} \approx 1.9$ Å, as obtained from extended x-ray absorption fine structure measurements (EXAFS).[84,85]

$BiFeO_3$ and $Bi_{0.5}Na_{0.5}TiO_3$ both possess a rhombohedrally distorted ABO_3-type perovskite structure at room temperature with the space group $R3c$. Thus the A-site cations, i.e., 100% Bi^{3+} in BFO and 50% Bi^{3+}/50% Na^+ in BNT, are 12-fold coordinated by oxygen anions. The Bi-O bond lengths for BFO and BNT determined using x-ray diffraction (XRD) and extended x-ray absorption fine structure (EXAFS) are 2.31 and 2.20 Å, respectively (see Table I).[87,89] The slightly smaller Bi-O bond length in BNT compared to BFO is related to the smaller ionic radius of Ti^{4+} compared to that of Fe^{3+} as well as due to the fact that in BNT half of the A-site positions are occupied by the smaller Na^+ ions. The Fe-O bond lengths in BFO are very close to the Fe-O bond length in Fe_2O_3 and therefore indicate a very similar Fe environment between these materials, which is corroborated by the XPS measurements.

B. Electronic structure

The molecular orbital interactions in Fe_2O_3 are characterized by a large exchange interaction leading to the high-spin d^5 configuration, which is the origin of the small energy gap of 2.1 eV.[78] The crystal field interaction of the Fe 3d orbitals leads to a subsequent splitting into t_{2g} and e_g states. In the distorted octahedral coordination of the iron atoms in Fe_2O_3 and $BiFeO_3$ the e_g states interact with the oxygen ligands and form bonding and antibonding states as illustrated in the left graph of Fig. 6. The states at the valence band maximum, which are fundamental for the absolute value of E_{VB}, do therefore get strong contributions from Fe 3d and O 2p orbitals. This is in line with density functional theory calculations.[74] Due to the interaction between the O 2p and Fe 3d states, one can expect that E_{VB} is significantly higher in energy compared to oxides where the valence band is composed mostly of O 2p states, which is in good agreement with electrochemical measurements.[13] The upward shift of the valence band maximum in Fe_2O_3 is similar to the p-d repulsion between O 2p and Cu 3d states in Cu_2O,[90] which also exhibits a higher valence band maximum energy.[17,23]

The electronic structure at the valence band maximum of Bi_2O_3 is governed by the interaction of the O 2p states with the Bi 6s and 6p states. Cations with an occupied s orbital in the last valence shell, such as Bi^{3+} in Bi_2O_3, $BiFeO_3$, and $Bi_{0.5}Na_{0.5}TiO_3$ [a comparable effect occurs for Pb^{2+} in Pb(Zr,Ti)O_3], which possesses an electronic configuration of

TABLE I. Summary of structure parameters of Fe_2O_3, Bi_2O_3, BFO, and BNT. The abbreviations ND, XRD, and EXAFS stand for neutron diffraction, x-ray diffraction and extended x-ray absorption fine structure, respectively.

	crystal structure	band gap (eV)	Bi coordination	Bi-O bond length (Å) ND	Bi-O bond length (Å) XRD	Bi-O bond length (Å) EXAFS	Fe coordination	Fe-O bond length (Å) ND	Fe-O bond length (Å) XRD	Fe-O bond length (Å) EXAFS
α-Fe_2O_3	corundum	2.1[78]	—	—	—	—	6-O			1.94/2.06[84] 1.95/2.12[85]
α-Bi_2O_3	monoclinic	2.5[77,86]	5-O	2.13–3.40[83]	2.08–3.25[82]		—	—	—	—
δ-Bi_2O_3	cubic	3.1[86]	6-O	2.45[83]			—	—	—	—
$BiFeO_3$	rhombohedral	2.8[28–30]	12-O		2.31[87]		6-O	1.95/2.11[88]	1.95/2.12[87]	
$Bi_{0.5}Na_{0.5}TiO_3$	rhombohedral	3.2[79]	12-O			2.2[89]	—	—	—	—

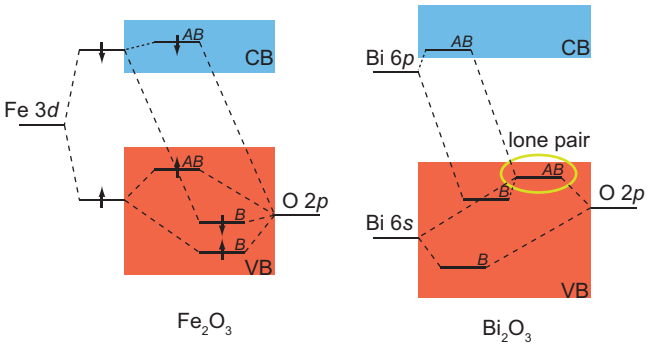

FIG. 6. (Color online) Molecular orbital diagram of Fe_2O_3 (left) and Bi_2O_3 (right). The left graph represents the octahedral coordination of Fe_2O_3. Only the bonding e_g states are illustrated and the nonbonding t_{2g} states are omitted. *B* and *AB* denote bonding and antibonding, respectively. The arrows illustrate the spin direction. Graph reproduced after Walsh,[75] Peng,[78] and Cox.[91]

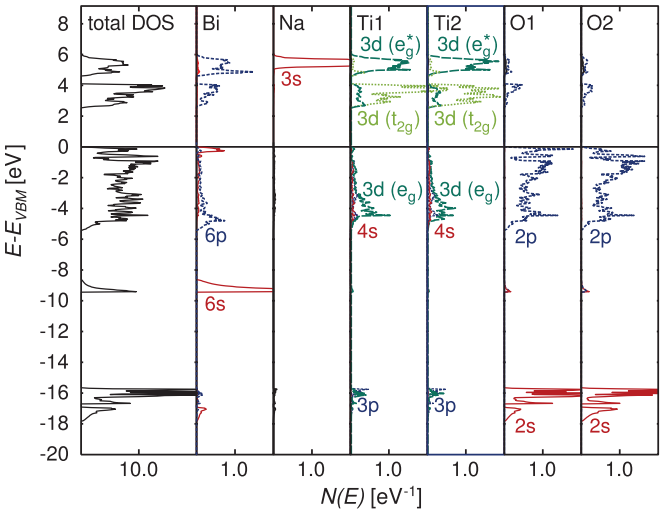

FIG. 7. (Color online) Density of states of $Bi_{0.5}Na_{0.5}TiO_3$. Partial densities of states are given per atom, the total density of states per primitive cell (2 f.u.).

$5d^{10}6s^26p^0$, prefers highly asymmetric coordination environment. This stereochemical distortion of the crystal structure corresponds to an asymmetric charge distribution.[92,93] The asymmetry is often referred to as "lone-pair"effect. Theoretical and experimental studies have demonstrated that the asymmetry can be attributed to the interaction between cation *s*, cation *p* and anion *p* orbitals.[92,94] Walsh and co-workers have revealed using DFT calculations and photoemission that in Bi-containing oxides the occupied cation $6s/6p$ orbital interact with the O $2p$ orbitals in a way that a bonding state at the bottom of the valence band and an antibonding state at the top of the valence band are formed.[26,75,77] The energetic situation is illustrated in the right graph of Fig. 6. Due to the distortion of the crystal lattice, the unoccupied cation $6p$ orbital hybridizes with the antibonding state which results from the interaction between the Bi $6s$ and the O $2p$ states. This coupling of the Bi $6p$ states leads to a stabilization of the occupied antibonding state accompanied by an asymmetric electron density and thus the formation of lone-pair orbital.[75] Similar effects have also been observed in other oxides containing As^{3+}, Sb^{3+}, and Sn^{2+}, which all have an $(n-1)d^{10}ns^2np^0$ configuration.[95,96] Although O $2p$ orbitals still provide the dominant contribution to the valence band states close to the Fermi level, the Bi $6s/6p$ orbitals exhibit a non-negligible contribution to these states.[96] The valence band maximum energy may therefore be significantly modified by this interaction.

The density of states of $Bi_{0.5}Na_{0.5}TiO_3$ is shown in Fig. 7. The calculated band gap amounts to 2.54 eV, in much better agreement with the experimental value of 3.3 eV[79] compared to a previous calculation.[93] A sharp contribution of Bi $6s$ states at the top and a broad contribution of Bi $6p$ states at the bottom of the upper valence band are evident. A similar sharp contribution of Bi $6s$ states to the topmost valence bands is also found for $BiFeO_3$.[74] The Bi $6s$ peak at the top of the BNT valence band is associated with a peak in the O1 partial density of states — the O1 atoms are located in the Bi planes — indicating Bi $6s,p$–O $2p$ hybridization, i.e., formation of a stereochemically active lone-pair orbital. The width of the upper valence band is also in agreement with the XPS measurements (see Fig. 3).

C. Band alignment

Schottky barrier heights obtained from electrical measurements of $SrRuO_3/BiFeO_3$/Pt capacitor structures have revealed a slight dependence of barrier height on interface orientation, i.e., barrier heights ranging from 0.62eV for (100) oriented films to 0.92 eV for (111) oriented films.[80] These values have been extracted from much smaller experimental barrier heights by adding the polarization contribution to the barrier height.[97] This procedure assumes that the screening of the polarization by the electrode does not depend on interface orientation. This is not necessarily the case as the screening depends critically on the interface configuration.[98–100] Theory has also predicted a dependence of barrier heights on surface termination, e.g., SrO versus TiO_2 surface termination of $SrTiO_3$.[101,102] However, photoemission experiments employing in-situ metal deposition onto contamination-free surfaces reproducibly reveal homogeneous barrier heights both for mixed-terminated and for polycrystalline materials,[2,54,57,103] indicating that no significant contribution of surface termination or interface orientation on barrier height.

However, ferroelectric polarization modifies the barrier height at an electrode interface.[97–100,104–106] The Schottky barrier heights measured for $BiFeO_3$ and $Bi_{0.5}Na_{0.5}TiO_3$ may be affected by ferroelectric polarization. A dependence of barrier height on polarization has been recently investigated quantitatively using XPS with *in situ* control of ferroelectric polarization.[106] These experiments indicated that the effect of polarization is not present right after electrode preparation but only after poling the sample. This can be explained either by a polarization which terminates either inside the material as suggested by Kretschmer and Binder,[107] or by the formation of closure-domains resulting in polarization parallel to the electrode interface.[108,109] Considering these observations, it seems justified to discuss Schottky barriers measured by XPS with *in situ* metal deposition onto clean surfaces in terms of

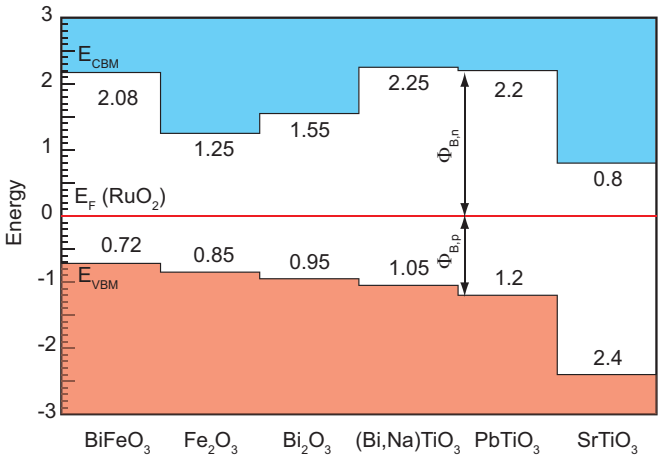

FIG. 8. (Color online) Energy band alignment of various oxides with respect to the Fermi level of RuO_2. The offsets at the energy of valence band maximum (E_{VBM}) are determined by aligning the barrier heights for holes ($\Phi_{B,p}$) and the offsets at the energy of conduction band minimum (E_{CBM}) are derived from the energy band gap correspondingly. The Fermi level of RuO_2 is set to 0 eV for a better clarity.

a unique band alignment without taking interface orientation, surface termination and ferroelectric polarization into account.

The Schottky barrier heights established at the contacts with RuO_2 can be used to align the valence band maxima with respect to each other. This procedure assumes transitivity of band alignment, i.e., that the alignment of energy bands between materials are additive. In particular, the valence band offsets between two oxides is obtained by subtracting their respective Schottky barrier heights with RuO_2, a procedure which has also been successfully applied with Au as a reference material.[110] The corresponding Schottky barriers and derived band alignments for Bi_2O_3, Fe_2O_3, $BiFeO_3$, and $Bi_{0.5}Na_{0.5}TiO_3$ are shown in Fig. 8. The energy levels of $PbTiO_3$ and $SrTiO_3$ from previous studies of interface formation with RuO_2[2] are included in the graph for comparison. The absence of interface reactions, a prerequisite for a reliable application of the transitivity rule, has been demonstrated above. Moreover, the validity of the transitivity rule for such interfaces has been demonstrated explicitly for STO and PTO,[2] providing further confidence that the procedure is appropriate. The transitivity of barrier heights at STO and PTO explicitly includes the interfaces with RuO_2. It is noted that the determined energy band alignment (see Fig. 8), and in particular, the Schottky barrier height at the BFO/RuO_2 interface, is quite different from that calculated using the charge neutrality levels by Robertson and Clark.[1,111] This deviation can be explained by the reduced density of induced gap states of ionic compounds.[51,112]

With respect to $SrTiO_3$, the valence band maxima of $PbTiO_3$ and all oxides investigated in this contribution are significantly higher in energy. The higher valence band maximum of Fe_2O_3 compared to STO concurs with electrochemical measurements.[13] It is also consistent with the observation that oxides without considerable cation contribution to the valence bands have very similar valence band maximum energies.[17] The higher E_{VB} of Bi_2O_3, Fe_2O_3, BFO, BNT, and PTO compared to STO are a clear manifestation of the cation contribution to the valence band states, which is negligible only in STO.[27] In Bi_2O_3, BNT, and PTO it can only be the antibonding cation 6*s* O 2*p* interaction stabilized by the cation 6*p* orbitals (see Sec. IV B), which is responsible for the higher valence band maximum compared to STO.

The higher valence band maximum of $BiFeO_3$ compared to $SrTiO_3$ is reasonable when compared to the electrical properties of these materials. While *n*-type conductivity, e.g., by Nb doping, can be easily achieved in STO,[113] recent studies showed that a *p*-type conductivity can be realized in BFO by substituting Bi with divalent acceptors such as Ca or Sr.[114,115] In addition, the conductivity of BFO is greatly reduced by substituting Fe with tetravalent or pentavalent donors such as Ti and Nb.[116–118] The electrical conductivities of BFO and STO do therefore agree with the requirement of a high E_{VB} for obtaining *p*-type conduction and a low E_{CB} for *n*-type conduction.[1–3]

The higher valence band maximum energy of Fe_2O_3 compared to that of $SrTiO_3$ and other oxides without significant cation contribution to the valence bands,[17] is evidently related to the contribution of the Fe 3*d* states, which are similar in energy as the O 2*p* states. The comparable E_{VB} of Bi_2O_3 and Fe_2O_3 suggests that the effect of the lone-pair orbital on the valence band maximum energy is as pronounced as that of the contribution of the Fe 3*d* states. This is somewhat surprising as, in contrast to the Fe 3*d* states, the overall contribution of the cation 6*s* and 6*p* states to the density of states in Bi_2O_3, $BiFeO_3$, and $Bi_{0.5}Na_{0.5}TiO_3$ is rather weak. Nevertheless, the effect of the lone-pair orbital on the valence band maximum is quite significant. This is particularly intriguing for BNT, where only 50% of the A sites are occupied by Bi atoms, leading to a contribution of Bi orbitals to the topmost states in the valence bands of less than ~5%, as evidenced by the DFT calculations (see Fig. 7).

Due to the similarity of E_{VB} of Bi_2O_3 and Fe_2O_3 it is not possible to directly discern from the experiment to which extent the lone-pair orbital and the Fe 3*d* states determine the valence band maximum energy in $BiFeO_3$. The experimental energy band alignment (see Fig. 8) implies that the lone-pair and the Fe 3*d* states does not lead to a significantly different valence band maximum energy compared to those of the parent binary oxides. These results indicate that the energies of the valence band maxima in these compounds can be derived from the local cation environments. The localized nature of the electronic states at the valence band maximum of BFO is consistent with a very small dispersion of the topmost valence bands.[111] The fact that the valence band maximum energy of BNT is comparable to those of BFO and Bi_2O_3 also suggests that the valence band states are strongly localized. In the case of extended bandlike states, narrower energy bands and therefore a lower E_{VB} are expected for BNT, as an influence of Na on the valence band maximum energy can safely be excluded (see Fig. 7 and Ref. 119). The direct correspondence of the valence band maximum energies with the local cation bonding environment may enable the estimation of valence band maximum energies of multinary compounds from their binary constituents.

Compared to Fe_2O_3 and Bi_2O_3, the valence band maximum of $BiFeO_3$ is 130 meV and 230 meV higher in energy,

respectively. It may hence be assumed that Fe 3*d* states are more important for E_{VB} in BFO than the Bi lone-pair orbital. According to DFT calculations, Fe 3*d* and Bi 6*s* states contribute approximately to the same extent to the total density of states of BFO near E_{VB}.[111] The comparison between Fe_2O_3, Bi_2O_3, and $Bi_{0.5}Na_{0.5}TiO_3$ shows, however, that this is not necessarily the most important factor. Additional argumentation is obtained by considering bond lengths and coordination numbers of the cations, which affect the crystal field splitting and therefore the energy separation between bonding and antibonding states in Fig. 6.[91] While the bond length and coordination of Fe are very similar in Fe_2O_3 and BFO (see Table I), the Bi ions in BFO exhibit shorter bond lengths and a higher coordination with oxygen than in δ-Bi_2O_3. Assuming that the local bonding environment determines the valence band maximum energy, this points towards a decisive influence of Bi states on the valence band maximum energy of BFO.

V. SUMMARY AND CONCLUSION

The Schottky barrier heights at the interfaces of Bi_2O_3, Fe_2O_3, $BiFeO_3$, and $Bi_{0.5}Na_{0.5}TiO_3$ with the high work function metallic RuO_2 have been determined by photoelectron spectroscopy using in-situ stepwise deposition of RuO_2. Interface formation revealed no chemical changes of the substrate during RuO_2 deposition and a upward band bending in all cases. The Schottky barrier heights for holes, i.e., the difference between the Fermi energy and the valence band maximum ($E_F - E_{VB}$) at the interface, are found to be 1.05 ± 0.15, 0.95 ± 0.1, 0.85 ± 0.1, and 0.72 ± 0.1eV for BNT, Bi_2O_3, Fe_2O_3, and BFO, respectively. The larger uncertainty for BNT is caused by the charging of the bare substrate surface, which makes the determination of the valence band maximum energy less accurate. The Schottky barriers are slightly smaller than that determined at the $PbTiO_3/RuO_2$ interface[51,57] but 1.35–1.7 eV larger than that determined at the $SrTiO_3/RuO_2$ interface.[50]

The different Schottky barrier heights, which provide a measure for the valence band maximum energy, have been discussed in terms of the different contributions to the electronic states in the valence band. Oxides where the valence bands are formed mainly by O 2*p* states, including $SrTiO_3$, show very similar valence band maximum energies as revealed by a series of interface experiments.[17] If, in contrast, cation states contribute significantly to the valence band, an upward shift of the valence band maximum results. Such contributions may originate from cation *d* orbitals as in the case of Fe_2O_3, but also from the lone-pair effect formed by the interaction of cation 6*s* and 6*p* orbitals with the O 2*p* orbitals. The latter give rise to the higher E_{VB} of Bi_2O_3, $Bi_{0.5}Na_{0.5}TiO_3$, $BiFeO_3$, and $PbTiO_3$.

The highest valence band maximum of the studied materials has been found for $BiFeO_3$. As the environment of Fe and the Fe-O bond length in BFO and Fe_2O_3 are comparable but the Bi-O bond length is reduced compared to Bi_2O_3, it is suggested that the Bi states are essential for the high valence band maximum in BFO. This is consistent with density of states calculations, which show a comparable contribution of Fe 3*d* and Bi 6*s*/6*p* states to the valence band maximum in BFO.[74,111] The considerable contribution of Bi 6*s*/6*p* states to the valence band maximum in BFO may lead to an enhanced carrier mobility compared to pure Fe_2O_3, as self-trapping leads to very low mobility in oxides with strong contribution of *d* states to the energy bands.[78]

The high valence band maximum of $BiFeO_3$ corresponds well with the observation of hole conduction in acceptor doped material,[114,115] while the high conduction band minimum agrees with the lack of *n*-type conduction in donor doped BFO.[116–118] As for the comparison between $SrTiO_3$ and $PbTiO_3$, this demonstrates once again that the energy band alignment can be used to rationalize the achievable electrical conductivity of materials, which indicates the importance of understanding energy band alignment. The present work demonstrates that band alignments determined experimentally using interface experiments with photoemission and in-situ sample preparation deviate significantly from theoretical predictions based on charge neutrality level calculations[1] and from band alignment determined electrochemically.[13] The agreement of Fermi level positions in $SrTiO_3$ and $PbTiO_3$ aligned according to the photoemission measurement[2] indicates that the alignment determined from photoemission experiments, which is measured at the intimate contact between solids, corresponds best with electrical properties of materials.

The comparison between Bi_2O_3, Fe_2O_3, $BiFeO_3$, and $Bi_{0.5}Na_{0.5}TiO_3$ suggests that the valence band maximum energy in oxides is largely determined by the local cation environment rather than by formation of extended energy band states. This provides a simple and rational way for manipulating the valence band maximum energy in oxides with multiple cations from the knowledge of the corresponding parent metal oxides.

ACKNOWLEDGMENTS

This work was supported by the German Science Foundation (DFG) within the collaborative research center SFB 595 (Electrical Fatigue of Functional Materials), the state of Hessen within the LOEWE center AdRIA (Adaptronik–Research, Innovation, Application), and the Romanian Ministry of Education, Research, Youth and Sport-National Authority for Scientific Research through the Idea-Complex Research Grant PN-II-ID-PCCE-2011-2-0006 (Contract No. 3/2012).

*sli@surface.tu-darmstadt.de

[1] J. Robertson and S. J. Clark, Phys. Rev. B **83**, 075205 (2011).
[2] R. Schafranek, S. Y. Li, F. Chen, W. B. Wu, and A. Klein, Phys. Rev. B **84**, 045317 (2011).
[3] A. Klein, J. Am. Ceram. Soc. **96**, 331 (2013).
[4] *Handbook of Transparent Conductors*, edited by D. S. Ginley, H. Hosono, and D. C. Paine (Springer, New York, 2010).
[5] G. H. Haertling, J. Am. Ceram. Soc. **82**, 797 (1999).

[6] J. Rödel, W. Jo, K. T. P. Seifert, E. Anton, T. Granzow, and D. Damjanovic, J. Am. Ceram. Soc. **92**, 1153 (2009).
[7] W. Walukiewicz, Physica B **302-303**, 123 (2001).
[8] A. Zunger, Appl. Phys. Lett. **83**, 57 (2003).
[9] P. Ágoston, C. Körber, A. Klein, M. J. Puska, R. M. Nieminen, and K. Albe, J. Appl. Phys. **108**, 053511 (2010).
[10] A. Zangwill, *Physics at Surfaces* (Cambridge University Press, Cambridge, 1988).
[11] A. Klein, C. Körber, A. Wachau, F. Säuberlich, Y. Gassenbauer, R. Schafranek, S. P. Harvey, and T. O. Mason, Thin Solid Films **518**, 1197 (2009).
[12] M. V. Hohmann, P. Ágoston, A. Wachau, T. J. M. Bayer, J. Brötz, K. Albe, and A. Klein, J. Phys.: Condens. Matter **23**, 334203 (2011).
[13] J. W. Schultze, Electrochim. Acta **45**, 3193 (2000), and Refs. 23–25 therein.
[14] S. Trasatti, Mater. Chem. Phys. **15**, 427 (1986).
[15] F. Capasso and G. Margaritondo, *Heterojunction Band Discontinuities* (North-Holland, Amsterdam, 1987).
[16] J. Waldrop, E. Kraut, S. Kowalczyk, and R. Grant, Surf. Sci. **132**, 513 (1983).
[17] A. Klein, Thin Solid Films **520**, 3721 (2012).
[18] S. H. Wei and A. Zunger, Appl. Phys. Lett. **72**, 2011 (1998).
[19] T. Schulmeyer, R. Hunger, M. Lebedev, W. Jaegermann, A. Klein, R. Kniese, and M. Powalla, Thin Solid Films **480**, 110 (2005).
[20] C. Tejedor and F. Flores, J. Phys. C **11**, L19 (1978).
[21] J. Tersoff, Phys. Rev. B **30**, 4874 (1984).
[22] W. Mönch, J. Vac. Sci. Technol. B **17**, 1867 (1999).
[23] J. Deuermeier, J. Gassmann, J. Brötz, and A. Klein, J. Appl. Phys. **109**, 113704 (2011).
[24] J. E. Jaffe and A. Zunger, Phys. Rev. B **29**, 1882 (1984).
[25] P. Pyykko, Chem. Rev. **88**, 563 (1988).
[26] D. J. Payne, R. G. Egdell, D. S. L. Law, P. A. Glans, T. Learmonth, K. E. Smith, J. H. Guo, A. Walsh, and G. W. Watson, J. Mater. Chem. **17**, 267 (2007).
[27] S. Piskunov, E. Heifets, R. I. Eglitis, and G. Borstel, Comput. Mater. Sci. **29**, 165 (2004).
[28] S. R. Basu, L. W. Martin, Y. H. Chu, M. Gajek, R. Ramesh, R. C. Rai, X. Xu, and J. L. Musfeldt, Appl. Phys. Lett. **92**, 091905 (2008).
[29] A. Kumar, R. C. Rai, N. J. Podraza, S. Denev, M. Ramirez, Y.-H. Chu, L. W. Martin, J. Ihlefeld, T. Heeg, J. Schubert, D. G. Schlom, J. Orenstein, R. Ramesh, R. W. Collins, J. L. Musfeldt, and V. Gopalan, Appl. Phys. Lett. **92**, 121915 (2008).
[30] J. F. Ihlefeld, N. J. Podraza, Z. K. Liu, R. C. Rai, X. Xu, T. Heeg, Y. B. Chen, J. Li, R. W. Collins, J. L. Musfeldt, X. Q. Pan, J. Schubert, R. Ramesh, and D. G. Schlom, Appl. Phys. Lett. **92**, 142908 (2008).
[31] J. Wang, J. B. Neaton, H. Zheng, V. Nagarajan, S. B. Ogale, B. Liu, D. Viehland, V. Vaithyanathan, D. G. Schlom, U. V. Waghmare, N. A. Spaldin, K. M. Rabe, M. Wuttig, and R. Ramesh, Science **299**, 1719 (2003).
[32] T. Zhao, A. Scholl, F. Zavaliche, K. Lee, M. Barry, A. Doran, M. P. Cruz, Y. H. Chu, C. Ederer, N. A. Spaldin, R. R. Das, D. M. Kim, S. H. Baek, C. B. Eom, and R. Ramesh, Nat. Mater. **5**, 823 (2006).
[33] Y. H. Chu, L. W. Martin, M. B. Holcomb, M. Gajek, S. J. Han, Q. He, N. Balke, C. H. Yang, D. Lee, W. Hu, Q. Zhan, P. L. Yang, A. Fraile-Rodriguez, A. Scholl, S. X. Wang, and R. Ramesh, Nat. Mater. **7**, 478 (2008).
[34] P. Fischer, M. Polomska, I. Sosnowska, and M. Szymanski, J. Phys. C: Solid State Physics **13**, 1931 (1980).
[35] M. Alexe and D. Hesse, Nat. Comm. **2**, 256 (2011).
[36] J. Seidel, D. Fu, S.-Y. Yang, E. Alarcón-Lladó, J. Wu, R. Ramesh, and J. W. Ager III, Phys. Rev. Lett. **107**, 126805 (2011).
[37] X. Xu, Y. H. Lin, P. Li, L. Shu, and C. W. Nan, J. Am. Ceram. Soc. **94**, 2296 (2011).
[38] Z. F. Bian, J. Zhu, S. H. Wang, Y. Cao, X. F. Qian, and H. X. Li, J. Phys. Chem. C **112**, 6258 (2008).
[39] L. F. Yin, J. F. Niu, Z. Y. Shen, and J. Chen, Environ. Sci. Technol. **44**, 5581 (2010).
[40] Z. Zhang, M. F. Hossain, and T. Takahashi, Mater. Lett. **64**, 435 (2010).
[41] H. Cheng, B. Huang, J. Lu, Z. Wang, B. Xu, X. Qin, X. Zhang, and Y. Dai, Phys. Chem. Chem. Phys. **12**, 15468 (2010).
[42] S. H. Hsieh, G. J. Lee, C. Y. Chen, J. H. Chen, S. H. Ma, T. L. Horng, K. H. Chen, and J. J. Wu, J. Nanosci. Nanotechnol. **12**, 5930 (2012).
[43] K. Sivula, F. Le Formal, and M. Grätzel, Chem. Sus. Chem. **4**, 432 (2011).
[44] M. Grätzel, Nature (London) **414**, 338 (2001).
[45] G. Smolenskii, V. A. Isupov, A. Agranovskaya, and N. Krainik, Sov. Phys. Solid State **2**, 2651 (1961).
[46] T. Takenaka and H. Nagata, J. Eur. Ceram. Soc. **25**, 2693 (2005).
[47] L. A. Schmitt, J. Kling, M. Hinterstein, M. Hoelzel, W. Jo, H.-J. Kleebe, and H. Fuess, J. Mater. Sci. **46**, 4368 (2011).
[48] W. Jo, J. E. Daniels, J. L. Jones, X. Tan, P. A. Thomas, D. Damjanovic, and J. Rödel, J. Appl. Phys. **109**, 014110 (2011).
[49] M. Otoničar, S. D. Škapin, M. Spreitzer, and D. Suvorov, J. Eur. Ceram. Soc. **30**, 971 (2010).
[50] R. Schafranek, J. Schaffner, and A. Klein, J. Eur. Ceram. Soc. **30**, 187 (2010).
[51] F. Chen, R. Schafranek, S. Li, W. B. Wu, and A. Klein, J. Phys. D: Appl. Phys. **43**, 295301 (2010).
[52] F. Chen, R. Schafranek, W. B. Wu, and A. Klein, J. Phys. D: Appl. Phys. **42**, 215302 (2009).
[53] F. Chen, R. Schafranek, W. B. Wu, and A. Klein, J. Phys. D: Appl. Phys. **44**, 255301 (2011).
[54] R. Schafranek, S. Payan, M. Maglione, and A. Klein, Phys. Rev. B **77**, 195310 (2008).
[55] C. Körber, S. P. Harvey, T. O. Mason, and A. Klein, Surf. Sci. **602**, 3246 (2008).
[56] M. Naderer, D. Schütz, T. Kainz, K. Reichmann, and F. Mittermayr, J. Eur. Ceram. Soc. **32**, 2399 (2012).
[57] F. Chen, R. Schafranek, A. Wachau, S. Zhukov, J. Glaum, T. Granzow, H. von Seggern, and A. Klein, J. Appl. Phys. **108**, 104106 (2010).
[58] G. Kresse and J. Hafner, Phys. Rev. B **47**, 558 (1993).
[59] G. Kresse and J. Hafner, Phys. Rev. B **49**, 14251 (1994).
[60] G. Kresse and J. Furthmüller, Comput. Mater. Sci. **6**, 15 (1996).
[61] G. Kresse and J. Furthmüller, Phys. Rev. B **54**, 11169 (1996).
[62] G. Kresse and D. Joubert, Phys. Rev. B **59**, 1758 (1999).
[63] P. E. Blöchl, Phys. Rev. B **50**, 17953 (1994).
[64] D. M. Ceperley and B. J. Alder, Phys. Rev. Lett. **45**, 566 (1980).
[65] H. J. Monkhorst and J. D. Pack, Phys. Rev. B **13**, 5188 (1976).
[66] J. F. Moulder, W. F. Stickle, P. E. Sobol, and K. D. Bomben, *Handbook of X-ray Photoelectron Spectroscopy* (Physical Electronics, Inc., Eden Prairie, 1995).
[67] G. C. Allen, M. T. Curtis, A. J. Hooper, and P. M. Tucker, J. Chem. Soc. Dalton Trans. (1974), 1525.
[68] R. P. Gupta and S. K. Sen, Phys. Rev. B **12**, 15 (1975).
[69] N. S. McIntyre and D. G. Zetaruk, Anal. Chem. **49**, 1521 (1977).

[70]P. Mills and J. L. Sullivan, J. Phys. D: Appl. Phys. **16**, 723 (1983).
[71]T. Fujii, F. M. F. de Groot, G. A. Sawatzky, F. C. Voogt, T. Hibma, and K. Okada, Phys. Rev. B **59**, 3195 (1999).
[72]C. R. Brundle, T. J. Chuang, and K. Wandelt, Surf. Sci. **68**, 459 (1977).
[73]R. J. Lad and V. E. Henrich, Phys. Rev. B **39**, 13478 (1989).
[74]A. T. Kozakov, K. A. Guglev, V. V. Ilyasov, I. V. Ershov, A. V. Nikol'skii, V. G. Smotrakov, and V. V. Eremkin, Phys. Solid State **53**, 41 (2011).
[75]A. Walsh, D. J. Payne, R. G. Egdell, and G. W. Watson, Chem. Soc. Rev. **40**, 4455 (2011).
[76]S. Doniach and M. Sunjic, J. Phys. C: Solid St. Phys. **3**, 285 (1970).
[77]A. Walsh, G. W. Watson, D. J. Payne, R. G. Edgell, J. H. Guo, P. A. Glans, T. Learmonth, and K. E. Smith, Phys. Rev. B **73**, 235104 (2006).
[78]H. Peng and S. Lany, Phys. Rev. B **85**, 201202 (2012).
[79]M. Bousquet, J. R. Duclere, E. Orhan, A. Boulle, C. Bachelet, and C. Champeaux, J. Appl. Phys. **107**, 104107 (2010).
[80]L. Pintilie, C. Dragoi, Y. H. Chu, L. W. Martin, R. Ramesh, and M. Alexe, Appl. Phys. Lett. **94**, 232902 (2009).
[81]D. Risold, B. Hallstedt, L. J. Gauckler, H. L. Lukas, and S. G. Fries, J. Phase Equilib. **16**, 223 (1995).
[82]G. Malmros, Acta Chem. Scand. **24**, 384 (1970).
[83]H. A. Harwig, Z. Anorg. Allg. Chem. **444**, 151 (1978).
[84]Z. H. Wu, L. Guo, Q. S. Li, and H. S. Zhu, J. Phys.: Condens. Matter **11**, 4961 (1999).
[85]C. M. Eggleston and M. F. Hochella, Am. Mineral. **77**, 911 (1992).
[86]V. P. Zhukov, V. M. Zhukovskii, V. M. Zainullina, and N. I. Medvedeva, J. Struct. Chem. **40**, 831 (1999), and Refs. 21 and 23 therein.
[87]R. Mazumder, P. S. Devi, D. Bhattacharya, P. Choudhury, A. Sen, and M. Raja, Appl. Phys. Lett. **91**, 062510 (2007).
[88]A. Palewicz, I. Sosnowska, R. Przenioslo, and A. W. Hewat, Acta Phys. Pol. A **117**, 296 (2010).
[89]P. A. Thomas, J. Kreisel, A. M. Glazer, P. Bouvier, Q. Z. Jiang, and R. Smith, Z. Kristall. **220**, 717 (2005).
[90]H. Raebiger, S. Lany, and A. Zunger, Phys. Rev. B **76**, 045209 (2007).
[91]P. A. Cox, *Transition Metal Oxides: An Introduction to Their Electronic Structure and Properties* (Oxford Clarendon Press, 1992).
[92]L. A. Olsen, J. Lopez-Solano, A. Garcia, T. Balic-Zunic, and E. Makovicky, J. Solid State Chem. **183**, 2133 (2010).
[93]M. Gröting, S. Hayn, and K. Albe, J. Solid State Chem. **184**, 2041 (2011).
[94]D. J. Payne, R. G. Egdell, A. Walsh, G. W. Watson, J. Guo, P. A. Glans, T. Learmonth, and K. E. Smith, Phys. Rev. Lett. **96**, 157403 (2006).
[95]A. Matsumoto, Y. Koyama, A. Togo, M. Choi, and I. Tanaka, Phys. Rev. B **83**, 214110 (2011).
[96]J. A. McLeod, R. J. Green, E. Z. Kurmaev, N. Kumada, A. A. Belik, and A. Moewes, Phys. Rev. B **85**, 195201 (2012).
[97]L. Pintilie, I. Vrejoiu, D. Hesse, G. LeRhun, and M. Alexe, Phys. Rev. B **75**, 104103 (2007).
[98]M. Stengel, D. Vanderbilt, and N. A. Spaldin, Phys. Rev. B **80**, 224110 (2009).
[99]M. Stengel, D. Vanderbilt, and N. A. Spaldin, Nat. Mater. **8**, 392 (2009).
[100]M. Stengel, P. Aguado-Puente, N. A. Spaldin, and J. Junquera, Phys. Rev. B **83**, 235112 (2011).
[101]J.-M. Albina, M. Mrovec, B. Meyer, and C. Elsässer, Phys. Rev. B **76**, 165103 (2007).
[102]M. Mrovec, J.-M. Albina, B. Meyer, and C. Elsässer, Phys. Rev. B **79**, 245121 (2009).
[103]Y. Segal, J. H. Ngai, J. W. Reiner, F. J. Walker, and C. H. Ahn, Phys. Rev. B **80**, 241107(R) (2009).
[104]E. Y. Tsymbal and H. Kohlstedt, Science **313**, 181 (2006).
[105]D. Lee, S. H. Baek, T. H. Kim, J.-G. Yoon, C. M. Folkman, C. B. Eom, and T. W. Noh, Phys. Rev. B **84**, 125305 (2011).
[106]F. Chen and A. Klein, Phys. Rev. B **86**, 094105 (2012).
[107]R. Kretschmer and K. Binder, Phys. Rev. B **20**, 1065 (1979).
[108]P. Aguado-Puente and J. Junquera, Phys. Rev. Lett. **100**, 177601 (2008).
[109]C.-L. Jia, K. W. Urban, M. Alexe, D. Hesse, and I. Vrejoiu, Science **331**, 1420 (2011).
[110]W. Mönch, J. Appl. Phys. **80**, 5076 (1996).
[111]S. J. Clark and J. Robertson, Appl. Phys. Lett. **90**, 132903 (2007).
[112]S. Kurtin, T. C. McGill, and C. A. Mead, Phys. Rev. Lett. **22**, 1433 (1969).
[113]M. V. Rozhdestvenskaya, I. T. Sheftel', V. A. Stogova, M. S. Kozyreva, and E. K. Krayukhina, Sov. Phys. Solid State **12**, 674 (1970).
[114]N. Maso and A. R. West, Chem. Mater. **24**, 2127 (2012).
[115]K. Brinkman, T. Iijima, and H. Takamura, Solid State Ionics **181**, 53 (2010).
[116]X. Qi, J. Dho, R. Tomov, M. G. Blamire, and J. L. MacManus-Driscoll, Appl. Phys. Lett. **86**, 062903 (2005).
[117]K. Kalantari, I. Sterianou, S. Karimi, M. C. Ferrarelli, S. Miao, D. C. Sinclair, and I. M. Reaney, Adv. Funct. Mater. **21**, 3737 (2011).
[118]Y. K. Jun, W. T. Moon, C. M. Chang, H. S. Kim, H. S. Ryu, J. W. Kim, K. H. Kim, and S. H. Hong, Solid State Commun. **135**, 133 (2005).
[119]M. Zeng, S. W. Or, and H. L. W. Chan, J. Appl. Phys. **107**, 043513 (2010).